

Threshold reduction in quantum cascade lasers with partially undoped, dual-wavelength interdigitated cascades

Axel Straub,^{a)} Trinesha S. Mosely,^{b)} Claire Gmachl,^{c)} Raffaele Colombelli, Mariano Troccoli, Federico Capasso, Deborah L. Sivco, and Alfred Y. Cho
Bell Laboratories, Lucent Technologies, 600 Mountain Avenue, Murray Hill, New Jersey 07974

(Received 29 November 2001; accepted for publication 28 February 2002)

A dual-wavelength quantum cascade (QC) laser with an interdigitated cascade is presented. Aside from providing two-wavelength operation at 8.0 and 9.5 μm wavelength, this laser design was used to test the role of extrinsic carriers in the injectors. An interdigitated cascade was grown with undoped injectors bridging 9.5 and 8.0 μm active regions, but doped injectors bridging 8.0 and 9.5 μm active regions. Clear laser action on both wavelengths demonstrates that doping of all injector regions is not a firm requirement for QC lasers. Comparison with a conventionally doped interdigitated cascade QC laser shows a threshold reduction by a factor of approximately 2 for the laser based on the active regions preceded by the undoped injector. This can be understood from the absence or strong reduction of impurity scattering related to the dopant ions. © 2002 American Institute of Physics. [DOI: 10.1063/1.1472473]

Quantum cascade (QC) lasers¹ have already reached a high level of maturity which is demonstrated by their good performance.^{1,2} The conventional QC laser consists of a semiconductor waveguide with an active core comprising a stack of alternating active regions and injectors. In the former, light is generated by electrons undergoing optical intersubband transitions in coupled quantum wells or short period superlattices. The latter provide electron transport between successive active regions. While it is customary that all active regions and injectors are identical, we have recently shown that this is not a firm requirement.³

In this letter, we investigate and question another commonly held principle, namely, that the injector requires doping. In fact, the early proposals of intersubband injection lasers⁴ did not include injectors or extrinsic carriers. As such, experimental demonstrations failed due to space charge injection, which did not allow a uniform electric field to be applied across the structure. As a result, the first demonstration of the QC laser⁵ included injectors and extrinsic charges. However, even in the early stages of that work it was understood, that—while being seemingly necessary—the dopants do negatively affect some aspects of laser action. First, impurity scattering considerably broadens the gain spectrum,⁶ therefore increasing the threshold current density, and shortens the nonradiative scattering time of the upper laser level, thus reducing inversion. Second, free carrier absorption by the extrinsic carriers increases the waveguide loss, again raising the laser threshold.

Here we present a QC laser having a dual-wavelength interdigitated cascade, i.e., a stack of active regions and injectors designed for emission at one wavelength interleaved with a second stack emitting at a substantially different wavelength. In our case, the two active regions emitted at

two different wavelengths, 8.0 and 9.5 μm , and the two injectors were designed to either bridge the 8.0 μm active region to the 9.5 μm one, or vice versa. More importantly, in one sample one injector type was left undoped, while in the reference sample both injectors were conventionally doped.

We observe two-wavelength laser action for both samples, which clearly demonstrates that it is not an essential requirement for QC lasers that all injectors are doped. Moreover, the overall performance of the laser based on the active region preceded by the undoped injector was greatly improved, showing a reduction in threshold by a factor of ~ 2 compared to the same-wavelength laser with doped injectors. It is the dual-wavelength QC laser, which by virtue of the two wavelengths allows a straightforward evaluation of the doped (represented by one wavelength) versus undoped (represented by the other wavelength) injectors. However, the finding of threshold reduction may have impact in particular also on QC lasers with homogeneous cascades, with identical active regions but selectively undoped injectors; this work is underway.

The samples were grown by molecular beam epitaxy in the InGaAs/AlInAs material system lattice matched to InP substrate. For both structures a 650-nm-thick low-doped ($n \approx 5 \times 10^{16} \text{ cm}^{-3}$) InGaAs buffer layer was first grown on low-doped ($n \approx 2 \times 10^{17} \text{ cm}^{-3}$) InP substrate, which simultaneously acts as the bottom cladding. The active waveguide core consisted of a stack containing $N_p = 20$ periods. Each period contained two different active regions of the so-called “three well vertical transition” type⁷ emitting at 8.0 and 9.5 μm , respectively, interleaved with the corresponding injector regions. The overall stack has a thickness of 1.91 μm . In both structures the injector region preceding the 9.5 μm active region was doped in its center portion to a sheet density of $3.52 \times 10^{11} \text{ cm}^{-2}$. Only in the reference sample was the injector preceding the 8.0 μm active region also doped to a sheet density of $3.4 \times 10^{11} \text{ cm}^{-2}$. The active waveguide core was subsequently capped by 400 nm of low-doped InGaAs

^{a)}Present address: University of New South Wales, Sydney, Australia.

^{b)}Present address: Southern University and A&M College, Baton Rouge, LA.

^{c)}Electronic mail: cg@lucent.com

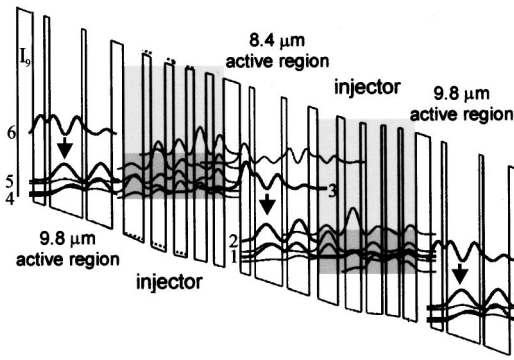


FIG. 1. Conduction band diagram and the moduli squared of the electron wave functions of three active regions with interleaved injectors calculated using iteratively Schrodinger's and Poisson's equations under an applied external electric field of 37 kV/cm. The dotted line indicates the correction to the band diagram if the injector preceding the 8.4 μm active region is left undoped. The laser transitions are indicated by the arrows. The nominal layer thicknesses in nanometers of one period from left to right starting from the first injection-barrier (I_0) are: 3.6/2.7/1.2/7.8/1.0/6.1/2.8/4.8/1.9/3.4/1.9/3.2/1.8/2.9/1.7/2.6/3.8/2.3/1.2/6.5/1.2/5.3/2.1/4.8/1.8/3.7/1.3/3.8/1.0/3.1/0.9/3.3. The underlined layers are Si doped in both samples to a density of $n \approx 4 \times 10^{17} \text{ cm}^{-3}$. In the reference sample the dotted underlined layers are also Si-doped to a density of $n \approx 4 \times 10^{17} \text{ cm}^{-3}$. The experimentally obtained peak wavelengths, 8.0 and 9.5 μm , are in reasonable agreement with the design wavelengths of 8.4 and 9.8 μm .

($n \approx 5 \times 10^{16} \text{ cm}^{-3}$), 2.9 μm of low-doped AlInAs (2.1 μm at $n \approx 1 \times 10^{17} \text{ cm}^{-3}$ followed by 800 nm at $n \approx 2 \times 10^{17} \text{ cm}^{-3}$), and 1 μm of high-doped ($n \approx 4 \times 10^{18} \text{ cm}^{-3}$) InGaAs. For the partially undoped (u) sample we estimate waveguide losses $\alpha_{w8,u}$ and $\alpha_{w9,u}$ of 21.5 and 21.7 cm^{-1} , for 8.0 and 9.5 μm wavelength, respectively. The corresponding, estimated waveguide losses of the reference sample (d) are $\alpha_{w8,d} = 26.9 \text{ cm}^{-1}$ and $\alpha_{w9,d} = 31.4 \text{ cm}^{-1}$, clearly larger than those of the partially undoped sample. Confinement factors $\Gamma_{8,u,d}$ and $\Gamma_{9,u,d}$ for the respective active regions are computed as 0.14 and 0.15, respectively. The effective refractive indices are calculated as $n_{\text{eff},8,d} \approx 3.29$, $n_{\text{eff},8,u} \approx 3.30$, and $n_{\text{eff},9,d} \approx n_{\text{eff},9,u} \approx 3.28$.

Figure 1 shows the conduction band diagram of one period of active regions with doped and undoped injectors calculated at the experimentally determined threshold electric field of 37 kV/cm. As can be seen, the difference in doping scheme does not significantly affect the band structure. The optical dipole matrix elements $z_{32,d}$ and $z_{32,u}$ for the 8.0 μm laser transition (between energy level "3" and "2") of the reference sample and the partially undoped sample are calculated as $z_{32,d} \approx z_{32,u} \approx 2.0 \text{ nm}$. For the 9.5 μm laser transition ("6" \rightarrow "5") they are computed as $z_{65,d} \approx z_{65,u} \approx 2.6 \text{ nm}$, respectively. Moreover the electron scattering times $\tau_{32,u} \approx \tau_{32,d}$ and $\tau_{65,u} \approx \tau_{65,d}$ as a result of LO phonon emission are calculated as 3.27 and 2.05 ps, respectively.⁸ The scattering lifetimes ($\tau_{2,u}$, $\tau_{5,u}$, $\tau_{2,d}$, and $\tau_{5,d}$) for electrons in the lower laser level are all calculated as $\approx 0.3 \text{ ps}$. The design energies of the optical transitions, $E_{32,u,d}$ ($= 148 \text{ meV} \equiv 8.4 \mu\text{m}$) and $E_{65,u,d}$ ($= 127 \text{ meV} \equiv 9.8 \mu\text{m}$), are in reasonable agreement with the measured values (8.0 and 9.5 μm).

Figure 2 shows a comparison of the luminescence spectra obtained at various current levels for the two samples measured from deep-etched, round mesas cleaved along the diameter, and with the light collected from the resulting

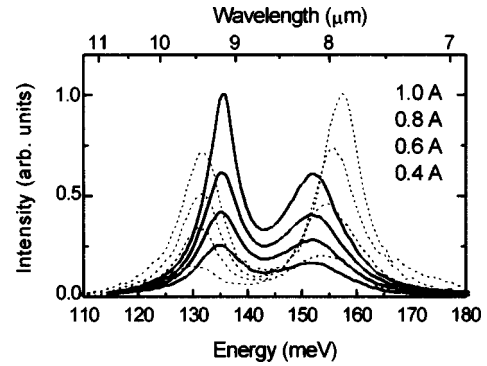


FIG. 2. Electroluminescence spectra of deep-etched, semicircle shaped mesas operated in pulsed mode at 10 K heat sink temperature and various peak current levels. The dashed and solid lines indicate the partially undoped and conventionally doped sample, respectively. The corresponding current densities are 2.5, 3.8, 5.1, and 6.4 kA cm^{-2} .

facet. The sets of spectra are normalized to the maximum intensity at a peak current level of 1 A. The small shifts of the peak wavelengths can be attributed to layer thickness variations. A clear difference in the overall shape of the spectra is observed between the two samples. While the reference sample displays the larger intensity at $\sim 9.5 \mu\text{m}$, the stronger emission of the partly undoped sample is at the 8.0 μm transition. The electroluminescence power at each wavelength is approximately proportional to $E_{32(65)} [\tau_{3(6)} / \tau_{\text{rad},32(65)}] N_p I \eta$, with $\tau_{3(6)}$ being the nonradiative scattering lifetime of the upper energy level, $\tau_{\text{rad},32(65)} (\gg \tau_{3(6)})$ its radiative scattering time, I is the current, and η is the collection efficiency. Thus, the reversal of the relative emission strengths with wavelength, i.e., the larger intensity of the 8.0 μm optical transition for the partly undoped sample indicates a significantly increased internal quantum efficiency [$\tau_{3(6)} / \tau_{\text{rad},32(65)}$] for the latter, resulting from an increased upper level scattering time, which is consistent with decreased impurity scattering.⁶ The full width at half maximum (FWHM) values were extracted from the luminescence measurements by fitting the sum of two Lorentzian lineshape functions to the data. The FWHM values $2\gamma_{32,u}$ and $2\gamma_{65,u}$ ($2\gamma_{32,d}$ and $2\gamma_{65,d}$) at a current level of 0.6 A were 9.5 and 7.9 meV (13.0 and 8.0 meV), respectively. One clearly sees the reduction in FWHM for the active regions preceded by the undoped injectors. Using the equations given in Ref. 7 and the experimentally obtained FWHM values the gain coefficients for the various wavelength lasers under the two doping schemes can be calculated as $g_{9,u} \approx g_{9,d} \approx 157 \text{ cm/kA}$ and $g_{8,u} \approx 143 \text{ cm/kA}$ and $g_{8,d} \approx 101 \text{ cm/kA}$.

Figure 3 shows the light output (L) and voltage (V) versus current (I) characteristics of two otherwise identical, doped and partially undoped QC lasers operated in pulsed mode at various heat-sink temperatures. The fact that the partially undoped sample displays laser action at both wavelengths clearly proves the viability of undoped injectors. Moreover, the slope efficiency of the partially undoped sample increases to 60 mW/A with respect to the reference sample (25 mW/A), which can only partly be explained with the reduced free carrier absorption and therefore reduced waveguide losses. Figure 3 also shows a laser spectrum displaying simultaneous two-wavelength emission and the typical Fabry-Perot modes of the as-cleaved laser.⁹

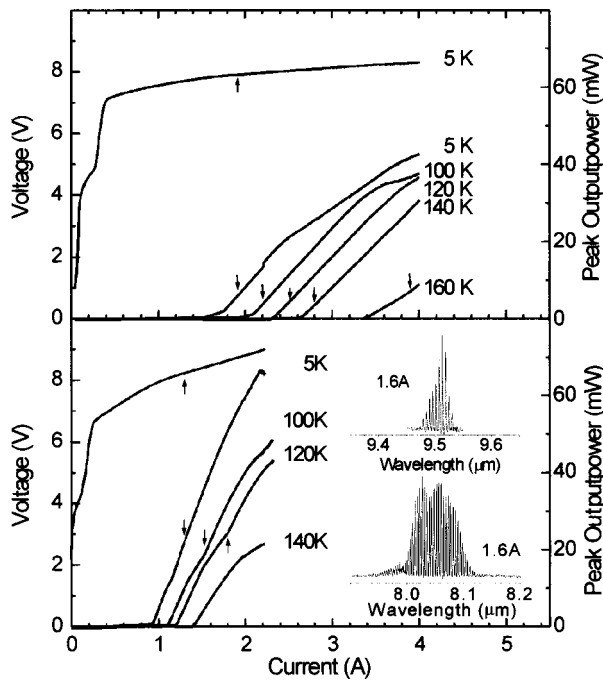


FIG. 3. Light output (L) and voltage (V) vs current (I) characteristics of pulsed operated, deep etched ridge waveguide lasers at various heat sink temperatures. Top: L - I - V characteristics of a reference laser (14 μm wide and 2.25 mm long). Bottom: L - I - V characteristics of the partially undoped laser (14 μm wide and 2.22 mm long). The arrows indicate the threshold of the corresponding second wavelength. The lasers were operated with 50 ns long current pulses at 84.2 kHz repetition rate. Insets: The insets show a spectrum of the partially undoped laser operated at 1.6 A.

Figure 4, finally, shows a comparison of the threshold current densities of the two samples and the two different wavelengths. Laser ridges with a width of 14–18 μm were cleaved to a length of 1.2, 2.25, and 3.2 mm. This results in mirror losses $\alpha_{m8,d} \approx \alpha_{m9,d} \approx \alpha_{m8,u} \approx \alpha_{m9,u}$ of 10.4, 5.6, and 3.9 cm^{-1} , respectively. Since the two wavelengths could not easily be separated during the L - I - V characterization measurements, the threshold currents were read from the real-time spectral monitor. The low temperature behavior of the threshold current densities of the reference sample can be understood from the calculated values. Using the estimated waveguide and mirror losses and the calculated gain coefficients, we expect a lower threshold current density (1.6 kA/cm^2 for a 2.25 mm long device) for the 9.5 μm radiation than for the 8.0 μm radiation (2.3 kA/cm^2). This trend is well reproduced in the experimental data (4.6 kA/cm^2 at 9.5 μm , vs 5.8 kA/cm^2 at 8.0 μm).

For the partially undoped structure—with its significantly larger gain for 8.0 μm radiation and the generally lower waveguide loss—we consequently expect a 45% reduction of the threshold current density for the 8.0 μm ra-

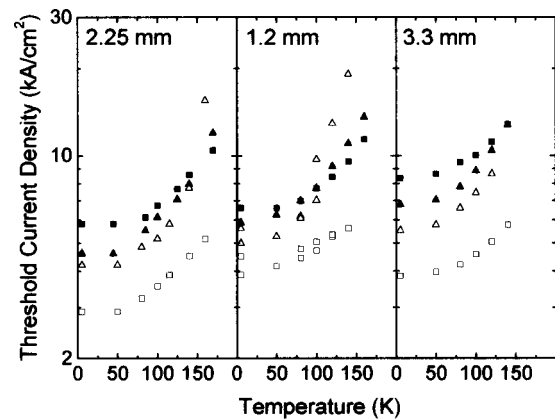


FIG. 4. Comparison of the threshold current densities of the two different samples at the two different wavelengths. The threshold current densities were measured for various-length lasers as indicated and versus heat sink temperature. Squares show the threshold current densities of the 8.0 μm radiation, and triangles indicate 9.5 μm emission, the conventionally doped sample is represented by the filled symbols, and the partially undoped sample by open symbols. The strong reduction in laser threshold for the QC-laser active regions preceded by the undoped injector (8.0 μm , $\blacksquare \rightarrow \square$) can clearly be seen and compared to the minor reduction for the conventionally doped QC laser (9.5 μm , $\blacktriangle \rightarrow \triangle$). The temperature behavior of the lasers can be understood from thermal backfilling (see Ref. 7).

diation and 20% reduction for the 9.5 μm radiation, respectively, over the values obtained for the conventionally doped sample. In fact, we observe a large reduction ($\sim 47\%$) in the threshold current density of the 8.0 μm emission (to 3.07 kA/cm^2) and only a minor one (13%) for the 9.5 μm emission (to 4.0 kA/cm^2).

The work was partly supported by DARPA/US ARO under Contract No. DAAD19-00-C-0096. A.S. acknowledges the support of the Studienstiftung des Deutschen Volkes.

- ¹F. Capasso, C. Gmachl, R. Paiella, A. Tredicucci, A. L. Hutchinson, D. L. Sivco, J. N. Baillargeon, A. Y. Cho, and H. C. Liu, *IEEE J. Sel. Top. Quantum Electron.* **6**, 931 (2000).
- ²D. Hofstetter, M. Beck, T. Aellen, J. Faist, U. Oesterle, M. Illegems, E. Gini, and H. Melchior, *Appl. Phys. Lett.* **78**, 1964 (2001).
- ³C. Gmachl, D. L. Sivco, J. N. Baillargeon, A. L. Hutchinson, F. Capasso, and A. Y. Cho, *Appl. Phys. Lett.* **79**, 572 (2001).
- ⁴R. F. Kazarinov and R. A. Suris, *Sov. Phys. Semicond.* **5**, 207 (1971).
- ⁵J. Faist, F. Capasso, D. L. Sivco, C. Sirtori, A. L. Hutchinson, and A. Y. Cho, *Science* **264**, 553 (1994).
- ⁶J. Faist, F. Capasso, C. Sirtori, D. L. Sivco, A. L. Hutchinson, S. N. G. Chu, and A. Y. Cho, *Appl. Phys. Lett.* **65**, 94 (1994).
- ⁷J. Faist, F. Capasso, C. Sirtori, D. L. Sivco, J. N. Baillargeon, A. L. Hutchinson, S. N. G. Chu, and A. Y. Cho, *Appl. Phys. Lett.* **68**, 3680 (1996).
- ⁸R. Ferreira and G. Bastard, *Phys. Rev. B* **40**, 1074 (1989).
- ⁹Multiwavelength operation in quantum cascade lasers has previously been reported in A. Tredicucci, C. Gmachl, F. Capasso, D. L. Sivco, A. L. Hutchinson, and A. Y. Cho, *Nature (London)* **396**, 350 (1998); C. Gmachl, D. L. Sivco, J. N. Baillargeon, A. L. Hutchinson, F. Capasso, and A. Y. Cho, *Appl. Phys. Lett.* **79**, 572 (2001).

Applied Physics Letters is copyrighted by the American Institute of Physics (AIP). Redistribution of journal material is subject to the AIP online journal license and/or AIP copyright. For more information, see <http://ojps.aip.org/aplo/aplcr.jsp>
Copyright of Applied Physics Letters is the property of American Institute of Physics and its content may not be copied or emailed to multiple sites or posted to a listserv without the copyright holder's express written permission. However, users may print, download, or email articles for individual use.